


## Unraveling the role of dangling bonds passivation in amorphous $Ga_2O_3$ for high-performance solar-blind UV detection

Zhengru Li(李正濡), Rui Zhu(朱锐), Huili Liang(梁会力), Shichen Su(宿世臣), and Zengxia Mei(梅增霞)
**Citation:**Chin. Phys. B, 2025, 34 (**7**): 078502. DOI: 10.1088/1674-1056/adc624
http://cpb.iphy.ac.cn; http://iopscience.iop.org/cpb

**What follows is a list of articles you may be interested in**

---

## Thickness effect on solar-blind photoelectric properties of ultrathin *β*-$Ga_2O_3$ films prepared by atomic layer deposition

Shao-Qing Wang(王少青), Ni-Ni Cheng(程妮妮), Hai-An Wang(王海安), Yi-Fan Jia(贾一凡), Qin Lu(陆芹), Jing Ning(宁静), Yue Hao(郝跃), Xiang-Tai Liu(刘祥泰), and Hai-Feng Chen(陈海峰)
Chin. Phys. B, 2023, 32 (**4**): 048502. DOI: 10.1088/1674-1056/ac8ce9

## Analysis of high-temperature performance of 4H-SiC avalanche photodiodes in both linear and Geiger modes

Xing-Ye Zhou(周幸叶), Yuan-Jie Lv(吕元杰), Hong-Yu Guo(郭红雨), Guo-Dong Gu(顾国栋), Yuan-Gang Wang(王元刚), Shi-Xiong Liang(梁士雄), Ai-Min Bu(卜爱民), and Zhi-Hong Feng(冯志红)
Chin. Phys. B, 2023, 32 (**3**): 038502. DOI: 10.1088/1674-1056/ac9820

## RF magnetron sputtering induced the perpendicular magnetic anisotropy modification in Pt/Co based multilayers

Runze Li(李润泽), Yucai Li(李予才), Yu Sheng(盛宇), and Kaiyou Wang(王开友)
Chin. Phys. B, 2021, 30 (**2**): 028506. DOI: 10.1088/1674-1056/abcf9d

## Perpendicular magnetization switching by large spin—orbit torques from sputtered $Bi_2Te_3$

Zhenyi Zheng(郑臻益), Yue Zhang(张悦), Daoqian Zhu(朱道乾), Kun Zhang(张昆), Xueqiang Feng(冯学强), Yu He(何宇), Lei Chen(陈磊), Zhizhong Zhang(张志仲), Dijun Liu(刘迪军), Youguang Zhang(张有光), Pedram Khalili Amiri, Weisheng Zhao(赵巍胜)
Chin. Phys. B, 2020, 29 (**7**): 078505. DOI: 10.1088/1674-1056/ab9439

## Transition of photoconductive and photovoltaic operation modes in amorphous $Ga_2O_3$-based solar-blind detectors tuned by oxygen vacancies

Yan-Fang Zhang(张彦芳), Xuan-Hu Chen(陈选虎), Yang Xu(徐阳), Fang-Fang Ren(任芳芳), Shu-Lin Gu(顾书林), Rong Zhang(张荣), You-Dou Zheng(郑有炓), Jian-Dong Ye(叶建东)
Chin. Phys. B, 2019, 28 (**2**): 028501. DOI: 10.1088/1674-1056/28/2/028501

---

# Unraveling the role of dangling bonds passivation in amorphous $Ga_2O_3$ for high-performance solar-blind UV detection

Zhengru Li(李正濡)[1,2], Rui Zhu(朱锐)[2,†], Huili Liang(梁会力)[2,3], Shichen Su(宿世臣)[1,‡], and Zengxia Mei(梅增霞)[2,3,§]

[1] *School of Electronic Science and Engineering (School of Microelectronics), South China Normal University, Foshan* 528225, *China*
[2] *Songshan Lake Materials Laboratory, Dongguan* 523808, *China*
[3] *Institute of Physics, Chinese Academy of Sciences, Beijing* 100190, *China*

(Received 8 March 2025; revised manuscript received 31 March 2025; accepted manuscript online 10 April 2025)

Low-cost and large-area uniform amorphous $Ga_2O_3$ (a-$Ga_2O_3$) solar-blind ultraviolet (UV) detectors have garnered significant attention in recent years. Oxygen vacancy ($V_O$) defects are generally considered as the predominant defects affecting the detector performance. Reducing $V_O$ concentration generally results in both low dark current and low photo current, significantly limiting further improvement of the photo-to-dark current ratio (PDCR) parameter. Herein, a delicately optimized atomic layer deposition (ALD) method is revealed having the capability to break through the trade-off in a-$Ga_2O_3$, achieving both low dark current and high photocurrent simultaneously. For a clear demonstration, a-$Ga_2O_3$ contrast sample is prepared by magnetron sputtering and compared as well. Combined tests are performed including x-ray photoelectron spectroscopy, photoluminescence, electron paramagnetic resonance and Fourier-transform infrared spectroscopy. It is found that ALD a-$Ga_2O_3$ has a lower $V_O$ concentration, but also a lower dangling bonds concentration which are strong non-irradiation recombination centers. Therefore, decrease of dangling bonds is suggested to compensate for the low optical gain induced by low $V_O$ concentration and promote the PDCR to $\sim 2.06 \times 10^6$. Our findings firstly prove that the dangling bonds also play an important role in determining the a-$Ga_2O_3$ detection performance, offering new insights for further promotion of a-$Ga_2O_3$ UV detector performance via dual optimization of dangling bonds and $V_O$.

**Keywords:** amorphous gallium oxide, magnetron sputtering, atomic layer deposition, ultraviolet detectors, dangling bonds

**PACS:** 85.60.Gz, 81.15.Gh, 73.61.Jc, 61.72.jd

**DOI:** 10.1088/1674-1056/adcb24 **CSTR:** 32038.14.CPB.adcb24

## 1. Introduction

Solar-blind ultraviolet (UV) (200 nm–280 nm) detectors have received widespread attention for their potential application in flame monitoring, corona detection, missile tracking and near-Earth communication.[1,2] With suitable band gap ($\sim$ 5 eV), stable chemical properties and regulative carrier concentration, $Ga_2O_3$ is an ideal material for fabricating solar-blind UV detectors.[3–7] Further, compared with high-temperature epitaxial growth of crystalline $Ga_2O_3$ thin films, amorphous $Ga_2O_3$ (a-$Ga_2O_3$) thin films can achieve low-cost large-area deposition on any substrates. Especially, some recent works have proved that a-$Ga_2O_3$ owns detection performance comparable to $\beta$-$Ga_2O_3$ counterpart.[8,9] These features position a-$Ga_2O_3$ as a suitable material for solar-blind UV detection.

Benefiting from appropriate growth rate and excellent surface roughness as well as uniformity,[10,11] radio frequency (rf) magnetron sputtering is the main method to deposit a-$Ga_2O_3$ thin films. Oxygen vacancy ($V_O$) defects are generally considered the primary defects in theses a-$Ga_2O_3$thin films. It has been widely accepted that $V_O$ acts as a double-edged sword in the a-$Ga_2O_3$ detectors: when the $V_O$ concentration is low, both the light and dark currents of the device would reduce; conversely, when the $V_O$ concentration is high, both the light and dark currents would increase.[12–14] As a result, it is difficult for a-$Ga_2O_3$ solar-blind UV detectors to simultaneously achieve high photocurrent and low dark current, greatly hindering the promotion of weak light detection abilities.

Some device structures have been designed and proposed to mitigate the double-edged sword of $V_O$. In three-terminal phototransistors, by working in negative gate voltage to deplete the channel, the dark current can be effectively suppressed while the photocurrent keeps at a high level.[15,16] However, this method hardly solves the common negative bias illumination stress (NBIS) effect causing slow detection rate and terrible stability.[17,18] Fabrication of heterojunctions

†Corresponding author. E-mail: zhurui@sslab.org.cn
‡Corresponding author. E-mail: shichensu@126.com
§Corresponding author. E-mail: zxmei@iphy.ac.cn

© 2025 Chinese Physical Society and IOP Publishing Ltd. All rights, including for text and data mining, AI training, and similar technologies, are reserved.

is also a common method to marginally suppress dark current by interface barrier and promote photocurrent by built-in electric field.[19–21] In addition, Zhu *et al*. innovatively constructed a $V_O$-rich a-$Ga_2O_3$/$V_O$-poor a-$Ga_2O_3$ doublelayer structure, achieving an ultra-high photo-to-dark current ratio (PDCR) ($> 10^9$) by employing a periodic bias-switching operation mode.[22] However, while these approaches solve the $V_O$ dilemma to a certain extent, they also increase the fabrication complexity and integration cost of the devices, without fundamentally addressing the issues inherent in the thin films themselves.

In contrast to a-$Ga_2O_3$ thin films fabricated by sputtering, some a-$Ga_2O_3$ thin films synthesized by atomic layer deposition (ALD) manifest high photocurrent, even under low $V_O$ concentration conditions.[23–25] However, this performance promotion cannot be reasonably explained from the perspective of $V_O$ considering the above-mentioned $V_O$'s double-edged sword role. Therefore, it is necessary to explore the internal mechanism of the promotion for a further manipulation of a-$Ga_2O_3$ detectors' performance.

In this work, we prepared the a-$Ga_2O_3$ thin films by ALD and sputtering and characterize them using x-ray photoelectron spectroscopy (XPS), photoluminescence (PL) spectroscopy, electron paramagnetic resonance (EPR) and Fourier-transform infrared spectroscopy (FTIR). The comparative results show the passivation of dangling bonds in a-$Ga_2O_3$ film deposited by ALD contributes to a high photo current. Interestingly, its lower $V_O$ concentration accounts for a low dark current as well. Finally, the solar-blind UV detectors based on the a-$Ga_2O_3$ (ALD) films were annealed under nitrogen atmosphere at 350 °C for an optimized interface contact and suppressed persistent photoconductivity (PPC) phenomenon, thereby further enhancing the detection performance.

## 2. Results and discussion

Firstly, the effect of deposition temperature on the film qualities has been investigated in thermal ALD growth process. A series of $Ga_2O_3$ films were prepared with 1000 cycles on quartz substrates at 250 °C, 300 °C, 350 °C, and 400 °C respectively. Ozone and triethylgallium are adopted as precursors where one cycle consisted of a 0.3-s triethylgallium exposure, a 30-s nitrogen purge, a 10-s ozone exposure, and a 30-s nitrogen purge. Figure 1 shows the structural, optical, and chemical characterization results, and Table 1 presents the key data of these $Ga_2O_3$ films. A characteristic peak originating from the quartz substrate is observed at 22° in Fig. 1(a), indicating the amorphous structure nature of $Ga_2O_3$ films. The transmittance spectroscopy in Fig. 1(b) illustrates that all a-$Ga_2O_3$ films exhibit distinct absorption in the solar-blind UV region. Moreover, the inset obtained by Tauc's method demonstrates that the band gap of a-$Ga_2O_3$ films increases from 4.80 eV to 5.02 eV as the growth temperature rises from 250 °C to 350 °C, suggesting more abundant oxidation status.

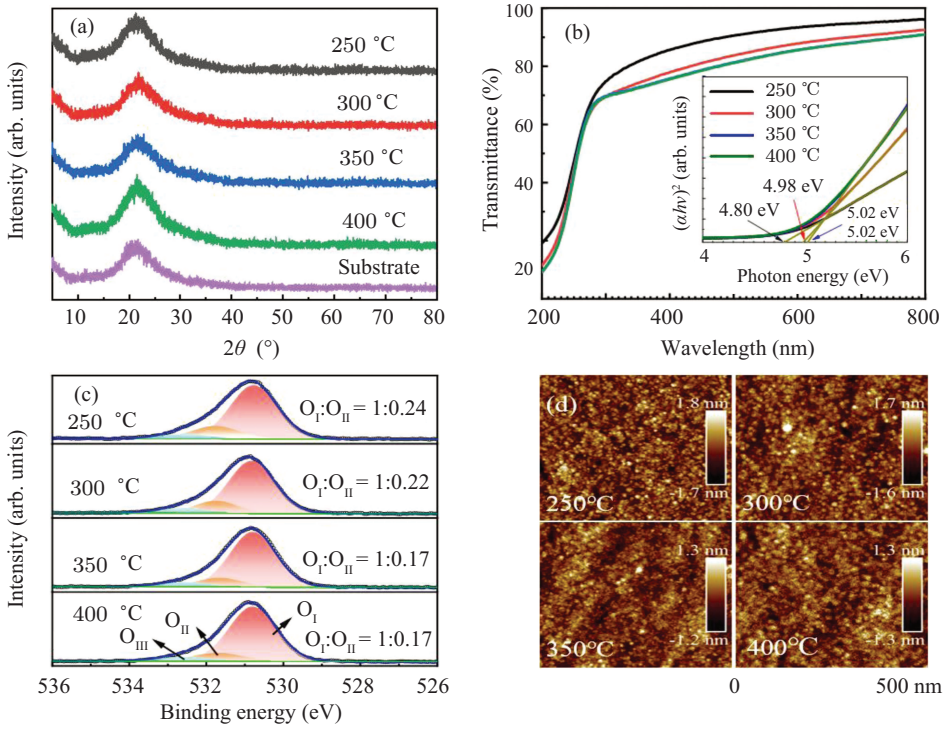



**Fig. 1.** Characteristics of $Ga_2O_3$ (ALD) films grown at different temperatures. (a) XRD curves, (b) transmittance spectra. The inset shows the plot of $(\alpha h\nu)^2$ versus $h\nu$ for these $Ga_2O_3$ (ALD) films. (c) O 1s core level spectra. (d) The A FM topography of these $Ga_2O_3$ (ALD) films surface.

To determine the chemical state of O element, the core level spectra of O 1s were measured by XPS and calibrated with C 1s peak (284.8 eV). As exhibited in Fig. 1(c), all the O 1s spectra can be fitted with three peaks centered at 530.8 eV, 531.7 eV, and 532.6 eV, which are named as $O_I$, $O_{II}$, and $O_{III}$, respectively. It has been recognized that $O_I$ peak corresponds to the lattice oxygen, $O_{II}$ peak is assigned to $V_O$, and $O_{III}$ peak is associated with hydroxyl and carbonyl species adsorbed on the film surface.[26–28] It is obvious that $V_O$ concentrations gradually decrease as the growth temperature rises from 250 °C to 350 °C, which can be inferred from the increasingly larger $O_I$:$O_{II}$ values (from 1:0.24 to 1:0.17). It means more abundant oxidation occurs. It should be noted that the band gap and $V_O$ concentration of a-$Ga_2O_3$ reach saturation above 350 °C. Combined with the fastest growth rate (41.88 nm/1000 cycles) shown in Table 1 and the smallest surface roughness (0.279 nm) shown in Fig. 1(d) at 350 °C, we can get that the Ga source can be completely oxidized, while an increased desorption rate leads to a decrease in growth rate and an increase in film roughness at temperatures above 350 °C. Therefore, we will only discuss a-$Ga_2O_3$ (ALD) film deposited at 350 °C in the following experiments.

**Table 1.** Comparisons of key data of $Ga_2O_3$ (ALD) films grown at different temperatures.

| Temperature (°C) | 250 | 300 | 350 | 400 |
|---|---|---|---|---|
| Thickness (nm) | 29.98 | 38.55 | 41.88 | 39.32 |
| $E_g$ (eV) | 4.80 | 4.98 | 5.02 | 5.02 |
| $O_I/O_{II}$ | 1:0.24 | 1:0.22 | 1:0.17 | 1:0.17 |
| Roughness (nm) | 0.385 | 0.369 | 0.279 | 0.285 |

In our previous works on sputtered a-$Ga_2O_3$ films the influence of oxygen flux on device performance has been explored in detail.[29,30] Because a-$Ga_2O_3$ (ALD) film has low $V_O$ concentration, for better comparison, we chose an oxygen flux of 1 sccm to deposit a-$Ga_2O_3$ film by sputtering in current work. In the following comparative experiments, a-$Ga_2O_3$ films prepared by ALD and sputtering are labeled as S1 and S2, respectively, while their thickness maintains ∼ 80 nm.

Firstly, planar metal–semiconductor–metal (MSM) UV detectors with Au (40 nm) Schottky contact are fabricated on S1 and S2, respectively. The schematics of device structure and the device photograph under an optical microscope are shown in Fig. 2(a). The detectors are equipped with interdigital electrodes consisting of 50 pairs of fingers, each 5 μm in width, 5 μm in spacing, and 150 μm in length as shown in Fig. 2(b). Figure 2(c) illustrates the *I*–*V* curves for S1 and S2 under dark and illumination of 254 nm (100 $\mu W \cdot cm^{-2}$). It can be apparently seen that the PDCR of S1 is much higher than that of S2. Taking 10-V bias voltage as an example, the dark current of S1 and S2 are $7.72 \times 10^{-13}$ A and $7.96 \times 10^{-14}$ A respectively, while the photo current are $1.59 \times 10^{-6}$ A and $9.97 \times 10^{-10}$ A, respectively. Therefore, the PDCR of S1 ($\sim 2.06 \times 10^6$) is over two orders of magnitude higher than that of S2 ($\sim 1.25 \times 10^4$). The time-dependent photo-response behaviors of S1 and S2 under a periodic 254-nm UV light illumination are shown in Fig. 2(d). Compared to S2, S1 exhibits obvious PPC effect, which can be solved in the following annealing process.

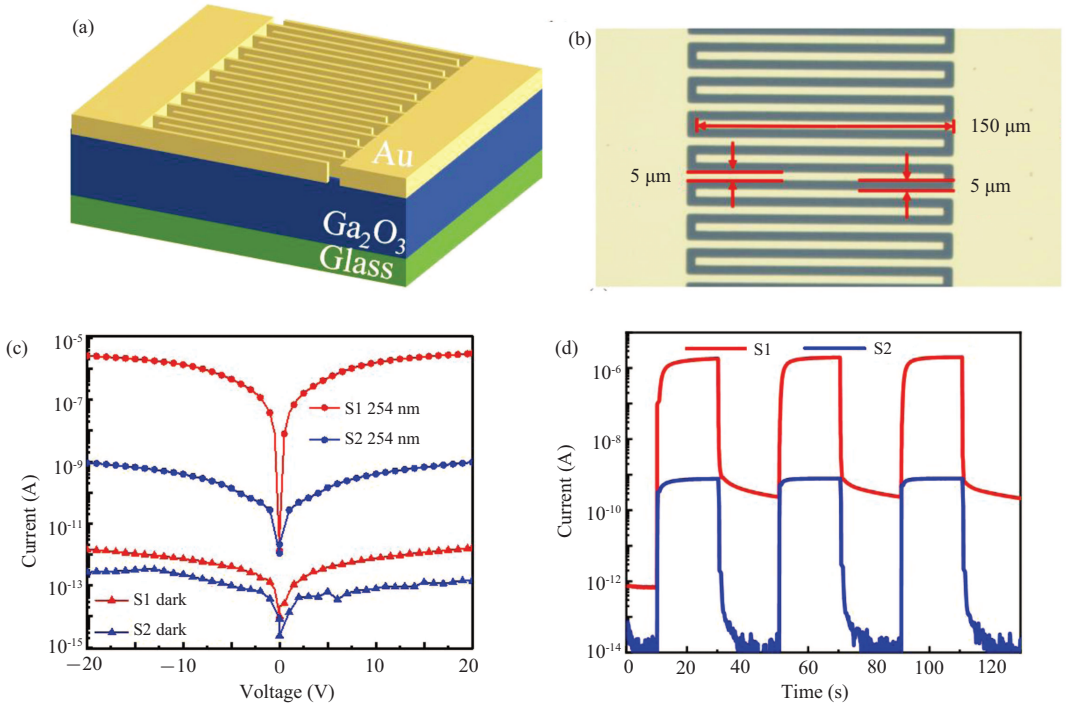



**Fig. 2.** The device structure and detection performance of S1 and S2. (a) The schematics of device structure and its magnified photograph under an optical microscope, (b) the interdigital electrode image under the microscope, (c) the *I*–*V* curves under 254-nm illumination and in dark, (d) transient response curves under periodic 254-nm UV light illumination.

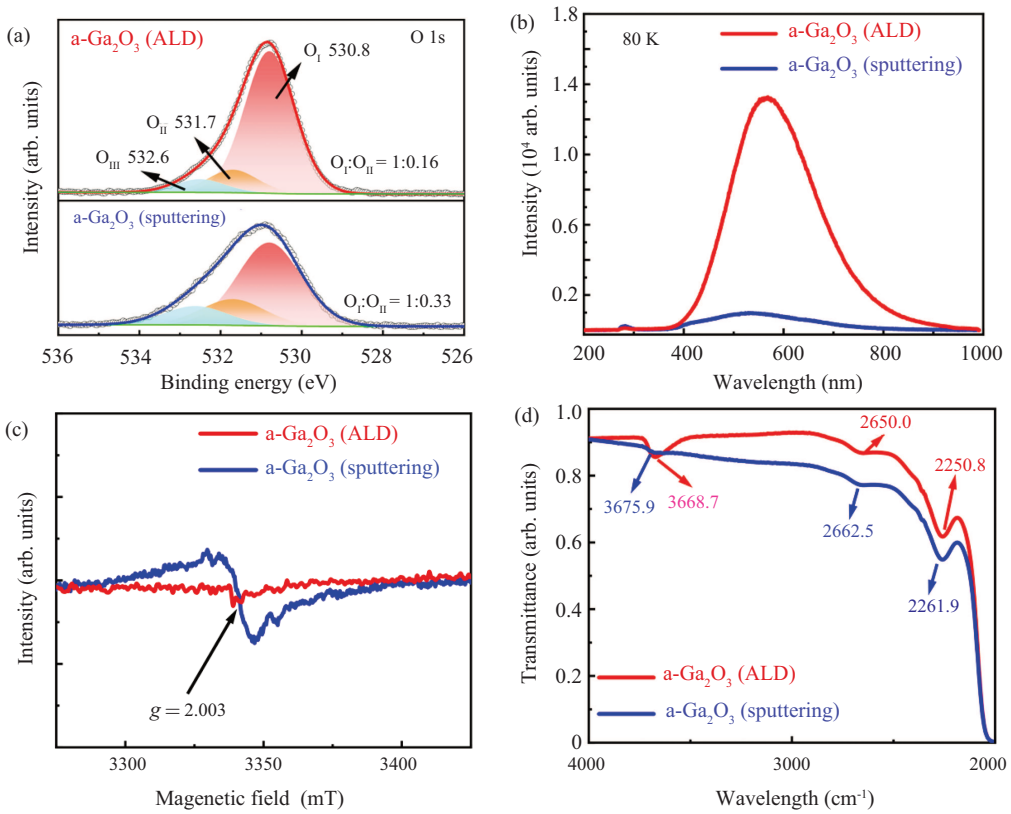



**Fig. 3.** The characterization results of sputtered a-$Ga_2O_3$ and a-$Ga_2O_3$(ALD): (a) XPS spectra of O 1s and fitting curves, (b) low-temperature PL spectra at 80 K, (c) EPR spectra at 10 K and 9.37 GHz, (d) FTIR spectra.

According to the role of the double-edged sword of $V_O$, the reason for the promoted PDCR of a-$Ga_2O_3$ (ALD) films cannot be explained merely from the perspective of $V_O$. To investigate the underlying factors causing the performance differences between S1 and S2, we performed a comprehensive characterization of the 80-nm sputtered a-$Ga_2O_3$ and ALD a-$Ga_2O_3$ films. We first compared the O 1s core-level spectra of the two a-$Ga_2O_3$ films, assessing the concentration of Vo defects. As shown in Fig. 3(a), the proportion of $O_{II}$ are 0.33 and 0.16 for sputtered a-$Ga_2O_3$ and a-$Ga_2O_3$ (ALD), respectively, when taking $O_I$ as 1. The $O_I/O_{II}$ ratio is significantly higher in the a-$Ga_2O_3$ (ALD) film, indicating a lower concentration of $V_O$ defects in this film. However, the PL observation seems contrary to the XPS results. As shown in Fig. 3(b), the PL curves excited with 257 nm at 80 K demonstrate an enhanced deep-level emission in a-$Ga_2O_3$ (ALD) sample. The intensity of the emission peak around 580 nm for a-$Ga_2O_3$(ALD) film is approximately ten times larger than that of the sputtered a-$Ga_2O_3$ film. This deep-level emission is usually assigned to $V_O$.[31–33] Considering a-$Ga_2O_3$ (ALD) film exhibits a lower concentration of $V_O$ than sputtered a-$Ga_2O_3$ film, it can be speculated that the former has much fewer non-radiative recombination centers than the latter.[34]

The EPR measurements were applied to unravel the origin of non-radiative recombination centers in a-$Ga_2O_3$ (ALD) films. Figure 3(c) shows the EPR spectra of sputtered a-$Ga_2O_3$ and a-$Ga_2O_3$ (ALD) films at 10 K and 9.37 GHz. The sputtered a-$Ga_2O_3$ film exhibits a distinct EPR signal at $g = 2.003$, while the a-$Ga_2O_3$ (ALD) film shows no noticeable signal. The intensity of the EPR signal is proportional to the number of unpaired electrons.[35,36] The signal strength indicates that the number of dangling bonds in sputtered a-$Ga_2O_3$ film is much larger than in a-$Ga_2O_3$ (ALD) film. Dangling bonds are generally considered as main non-radiative recombination centers, which explains why the PL intensity of a-$Ga_2O_3$ (ALD) film is significantly higher than that of sputtered a-$Ga_2O_3$ film. The FTIR spectra of sputtered a-$Ga_2O_3$ and a-$Ga_2O_3$ (ALD) films are shown in Fig. 3(d). The curve of sputtered a-$Ga_2O_3$ exhibits broad bands at 2662 $cm^{-1}$ and 3676 $cm^{-1}$ and a sharp peak at 2262 $cm^{-1}$. The a-$Ga_2O_3$ (ALD) curve shows a broad band at 2650 $cm^{-1}$ and sharp peaks at 2251 $cm^{-1}$ and 3669 $cm^{-1}$. Three peaks are observed in both samples, which can be attributed to O–H stretching vibrations.[37–39] The intensities of all three peaks in the a-$Ga_2O_3$ (ALD) are stronger than those in the sputtered a-$Ga_2O_3$, indicating a higher O–H density in the a-$Ga_2O_3$ (ALD) film. The presence of O–H bonds in the films likely serves to passivate dangling bonds. Based on the above comprehensive characterization results, we believe that low dangling bonds density and low $V_O$ concentration contribute to the much higher PDCR in S1. Low dangling bonds density in a-$Ga_2O_3$ (ALD) film may originate from the self-limit growth

of ALD and the passivation of H from triethylgallium, which requires further research in the future.[40,41]

As mentioned above, S1 exhibits an obvious PPC effect as shown Fig. 2(c). To improve its time-response property, we employed two different annealing treatments to investigate their impact on the detectors' performance. The first one involved annealing the a-$Ga_2O_3$ (ALD) films in a nitrogen atmosphere at 350 °C for 30 minutes, followed by the deposition of electrodes and the fabrication of device, labeled S1′. The second is to anneal the final device under the same conditions, labeled S1″. Figure 4(a) shows the *I*–*V* curves measured before and after annealing. Taking 10-V bias voltage as an example, the dark current of S1, S1′, and S1″ are $7.72 \times 10^{-13}$ A, $2.97 \times 10^{-12}$ A, and $8.15 \times 10^{-14}$ A respectively, while the photo current are $1.59 \times 10^{-6}$ A, $3.53 \times 10^{-8}$ A, and $2.61 \times 10^{-7}$ A respectively. Therefore, S1″ exhibits the highest PDCR, with a value of $3.20 \times 10^{6}$. Time-dependent photoresponse behavior of S1, S1′, and S1″ under a periodic 254-nm UV light illumination is shown in Fig. 4(b). The PPC of S1′ hardly changes compared to S1, while the PPC phenomenon of S1″ is notably depressed The only difference between S1′ and S1″ is the sequence of annealing, with the former occurring before the fabrication of the device and the latter after. It indicates that the interface of S1″ has been modified through annealing. Moreover, in contrast to S1, both the increased dark current and decreased photocurrent decrease suggest the possibly increased dangling bonds in S1′. As we discussed in the FTIR spectra, low dangling bond density may benefit from the self-limit growth of ALD and the passivation of H. The direct annealing of S1 may induce the dissociation and escape of H, which counts for the above-mentioned results. Contrarily, the deposition of electrodes on S1 before annealing can mostly reserve the passivation effect and promote the Schottky barrier quality between Au and $Ga_2O_3$. Therefore, it is observed that the dark current and photocurrent in S1″ slightly decrease combined with the obviously suppressed PPC.

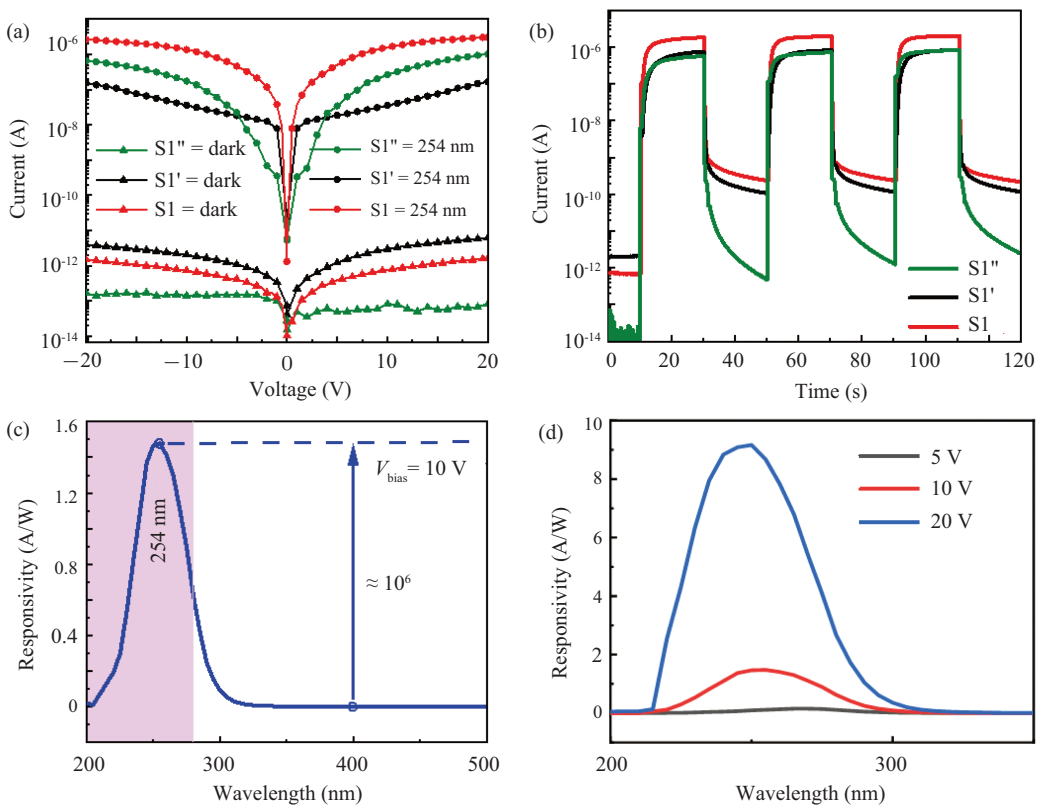



**Fig. 4.** Photoelectric performance characterization of a-$Ga_2O_3$ (ALD) UV detectors.(a) *I*–*V* curves of devices S1, S1′, and S1″ under 254-nm illumination and in dark. (b) Transient response curves of devices S1, S1′, and S1″ under 254-nm illumination. (c) Response spectrum of S1″. (d) Response spectrum of S1″ at different operating voltages.

**Table 2.** Key performance comparison of the a-$Ga_2O_3$ solar-blind UV detectors mentioned in this work. The working voltages are all kept at 10 V.

| Samples | $I_{254}$ | $I_{dark}$ | $I_{254}/I_{dark}$ | $R$ (A/W) | $R_{254}/R_{400}$ |
|---|---|---|---|---|---|
| S1 | $3.90 \times 10^{-10}$ | $7.96 \times 10^{-14}$ | $4.99 \times 10^{3}$ | $5.24 \times 10^{-3}$ | $2.58 \times 10^{4}$ |
| S2 | $1.59 \times 10^{-6}$ | $7.72 \times 10^{-13}$ | $2.06 \times 10^{6}$ | 7.15 | $2.20 \times 10^{5}$ |
| S2′ | $3.53 \times 10^{-8}$ | $2.97 \times 10^{-12}$ | $1.19 \times 10^{4}$ | $1.93 \times 10^{-1}$ | $7.20 \times 10^{5}$ |
| S2″ | $2.61 \times 10^{-7}$ | $8.15 \times 10^{-14}$ | $3.20 \times 10^{6}$ | 1.50 | $1.05 \times 10^{6}$ |

Since S1″ exhibits the optimal performance, we will focus on the other characteristic parameters of S1″ in the following discussion. Figure 4(c) shows the response spectra of S1″ under 254-nm illumination at 10 V, with an R254/R400 rejection ratio greater than $10^6$. R254 and R400 represent the device responsivity under illumination at 254 nm and 400 nm, respectively and the rejection ratio as high as $10^6$ demonstrates a superior solar-blind detection ability. Figure 4(d) presents the specific responsivity under 254-nm illumination for S1″ at bias voltages of 5 V, 10 V, and 20 V, with responsivities of 0.13, 1.50, and 8.80 A/W, respectively. It suggests that the detection performance can be further improved by increasing working voltage. Finally, we summarize all key device parameters for a-$Ga_2O_3$ solar-blind UV detectors mentioned in this work in Table 2. Benefitting from optimized ALD deposition method and annealing promotion of interface, S1″ exhibits the best performance in this work.

## 3. Conclusion

In summary, a comprehensive investigation reveals that the high PDCR in a-$Ga_2O_3$(ALD) films derives from both low $V_O$ concentration and low dangling bonds density. Low dangling bond density may benefit from the self-limit growth of ALD and the passivation of H. It is the decrease of dangling bonds that compensates for the low optical gain induced by low $V_O$ concentration. Moreover, the Au/$Ga_2O_3$ interface quality is promoted via annealing, which significantly contributes to a greatly suppressed PPC. Finally, we get an a-$Ga_2O_3$ solar-blind UV detector with excellent performance. Our study offers new sight for the route to promotion of PDCR in a-$Ga_2O_3$ solar-blind UV detector.

## Acknowledgments

Project supported by the National Natural Science Foundation of China (Grant Nos. 62404146, 12174275, and 62174113), the Basic and Applied Basic Research Foundation of Guangdong Province, China (Grant Nos. 2023A1515110730 and 2023A1515140094), and the INTPART Program at the Research Council of Norway (Project number 322382).

## References

[1] Zheng W, Huang F, Zheng R and Wu H 2015 *Adv. Mater.* **27** 3921
[2] Zheng W, Lin R, Ran J, Zhang Z, Ji X and Huang F 2018 *ACS Nano* **12** 425
[3] Zheng X Q, Lee J, Rafique S, Han L, Zorman C A, Zhao H and Feng P X L 2017 *ACS Appl. Mater. Interfaces* **9** 43090
[4] Zhao B, Wang F, Chen H, Zheng L, Su L, Zhao D and Fang X 2017 *Adv. Funct. Mater.* **27** 1700264
[5] Kong W Y, Wu G A, Wang K Y, Zhang T F, Zou Y F, Wang D D and Luo L B 2016 *Adv. Mater* **28** 10725
[6] Lin R, Zheng W, Zhang D, Zhang Z, Liao Q, Yang L and Huang F 2018 *ACS Appl. Mater. Interfaces* **10** 22419
[7] Qian L X, Wang Y, Wu Z H, Sheng T and Liu X Z 2017 *Vacuum* **140** 106
[8] Cui S, Mei Z, Zhang Y, Liang H and Du X 2017 *Adv. Opt. Mater.* **5** 1700454
[9] Qian L X, Wu Z H, Zhang Y Y, Lai P T, Liu X Z and Li Y R 2017 *ACS Photonics* **4** 2203
[10] Zhao Q C, Hao R T, Liu S J, Liu X X, Chang F R, Yang M, Lu Y L and Wang S R 2017 *Acta Phys. Sin.* **66** 226801 (in Chinese)
[11] Wang Y, Wang M, Shen L, Zhu Y, Sun X, Shi G, Xu X, Li R and Ma W 2018 *Chin. Phys. B* **27** 017801
[12] Hu S, Han D, Jiang K, Liu N, Wang W, Zhang J, Liu K, Zhang T, Zhang W and Ye J 2023 *Appl. Phys. Express* **16** 021005
[13] Wang G, Wang H, Chen T, Feng Y, Zeng H, Guo L, Liu X and Yang Y 2023 *Nanotechnology* **35** 095201
[14] Zhang Y F, Chen X H, Xu Y, Ren F F, Gu S L, Zhang R, Zheng Y D and Ye J D 2019 *Chin. Phys. B* **28** 028501
[15] Han Z, Liang H, Huo W, Zhu X, Du X and Mei Z 2020 *Adv. Opt. Mater.* **8** 1901833
[16] Shi Y, Shiah Y S, Sim K, Sasase M, Kim J and Hosono H 2022 *Appl. Phys. Lett.* **121** 212101
[17] Chang H Y, Chang T C, Tai M C, Huang B S, Zhou K J, Wang Y B, Kuo H M and Huang J W 2023 *Appl. Phys. Lett.* **122** 123504
[18] Kiazadeh A, Gomes H L, Barquinha P, Martins J, Rovisco A, Pinto J V, Martins R and Fortunato E 2016 *Appl. Phys. Lett.* **109** 051606
[19] Yu J, Javaid K, Liang L, Wu W, Liang Y, Song A, Zhang H, Shi W, Chang T C and Cao H 2018 *ACS Appl. Mater. Interfaces* **10** 8102
[20] Chen W H, Ma C H, Hsieh S H, Lai Y H, Kuo Y C, Chen C H, Chang S P, Chang S J, Horng R H and Chu Y H 2022 *ACS Appl. Electron. Mater.* **4** 3099
[21] Qi X, Ji X, Yue J, Qi S, Wang J, Li P and Tang W 2022 *Crystals* **12** 1284
[22] Zhu R, Liang H, Bai H, Zhu T and Mei Z 2022 *Appl. Mater. Today* **29** 101556
[23] Hsu C H, Zhu R F, Kang P C, Gao P, Wu W Y, Wuu D S, Lien S Y and Zhu W Z 2023 *Mater. Lett.* **340** 134204
[24] Yang Y, Liu W, Huang T, Qiu M, Zhang R, Yang W, He J, Chen X and Dai N 2021 *ACS Appl. Mater. Interfaces* **13** 41802
[25] Amsterdam S H, Mane A U and Martinson A B F 2023 *ACS Appl. Electron. Mater.* **5** 5962
[26] Russo P, Xiao M, Liang R and Zhou N Y 2018 *Adv. Funct. Mater.* **28** 1706230
[27] Liao Y, Xie Z, Song H, Xue J and Tan C K 2024 *Appl. Phys. Lett.* **125** 192106
[28] Liang H, Cui S, Su R, Guan P, He Y, Yang L, Chen L, Zhang Y, Mei Z and Du X 2019 *ACS Photonics* **6** 351
[29] Liang H, Han Z and Mei Z 2021 *Physica Status Solidi (a)* **218** 2000339
[30] Zhu R, Liang H, Hu S, Wang Y and Mei Z 2022 *Adv. Elect. Materials* **8** 2100741
[31] Oda H, Kimura N, Yasukawa D, Wakai H and Yamanaka A 2017 *Physica Status Solidi (a)* **214** 1600670
[32] Onuma T, Nakata Y, Sasaki K, Masui T, Yamaguchi T, Honda T, Kuramata A, Yamakoshi S and Higashiwaki M 2018 *J. Appl. Phys.* **124** 075103
[33] Cooke J, Ranga P, Jesenovec J, McCloy J S, Krishnamoorthy S, Scarpulla M A and Sensale-Rodriguez B 2022 *Sci. Rep.* **12** 3243
[34] Zi L, Heng Z, Hao W and Chang L 2019 *Acta Phys. Sin.* **68** 107301 (in Chinese)
[35] Ding K, Zhang H, Jiang J, Luo J, Wu R, Ye L, Tang Y, Pang D, Li H and Li W 2024 *Adv. Sci.* **11** 2407822
[36] Wili N 2023 *Journal of Magnetic Resonance Open* **16** 100108
[37] Vimont A, Lavalley J C, Sahibed-Dine A, Otero Areán C, Rodríguez Delgado M and Daturi M 2005 *J. Phys. Chem. B* **109** 9656
[38] Yang J (Jeanne), Zhao Y and Frost R L 2009 *Spectrochimica Acta Part A: Molecular and Biomolecular Spectroscopy* **74** 398
[39] Kazansky V B, Subbotina I R, Pronin A A, Schl?gl R and Jentoft F C 2006 *J. Phys. Chem. B* **110** 7975
[40] Hou C X, Zheng X H, Jia R, Tao K, Liu S J, Jiang S, Zhang P F, Sun H C and Li Y T 2017 *Chin. Phys. B* **26** 098103
[41] Chang A, Mao Y, Huang Z, Hong H, Xu J, Huang W, Chen S and Li C 2020 *Chin. Phys. B* **29** 038102